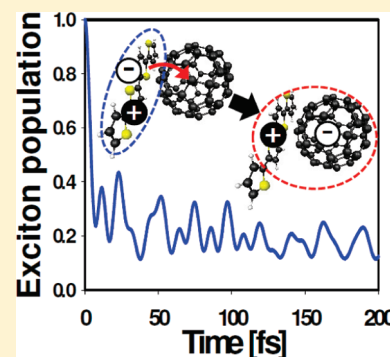


Exciton Dissociation at Thiophene/Fullerene Interfaces: The Electronic Structures and Quantum Dynamics

Hiroyuki Tamura,^{*,†} Irene Burghardt,^{‡,§} and Masaru Tsukada[†][†]WPI-Advanced Institute for Material Research, Tohoku University, 2-1-1 Katahira, Aoba-ku, Sendai, 980-8577, Japan[‡]Département de Chimie, Ecole Normale Supérieure, 24 rue Lhomond, F-75231 Paris cedex 05, France

ABSTRACT: Exciton dissociation at donor–acceptor heterojunctions is one of the key processes that determine the energy conversion efficiency of organic solar cells. Here, we theoretically investigate the exciton dissociations at oligothiophene/C₆₀ donor–acceptor heterojunctions by using the long-range corrected time-dependent density functional theory and quantum dynamics calculations. We analyze the absorption spectra, electronic structures in adiabatic and diabatic representations, vibronic coupling, and dynamics of the exciton dissociations. The coupling strength and relative energy between the exciton and charge transfer (CT) states depend sensitively on the donor–acceptor distance and the stacking structure, which in turn affects the absorption spectra and the dynamics of exciton dissociations. Our quantum dynamics calculations exhibit ultrafast exciton dissociations owing to the strong coupling between the exciton and CT states, as observed in the time-resolved spectroscopies of the donor–acceptor interfaces of conjugated polymers and fullerenes.



1. INTRODUCTION

Organic solar cells are promising next-generation photovoltaics owing to their potential for cost-effective energy sources, so that great efforts have been devoted to the development of high-efficiency organic solar cells.^{1–13} At present, relatively high conversion efficiencies have been reported for donor–acceptor bulk heterojunctions consisting of conjugated polymers and fullerenes (Figure 1a,b),^{1–4} namely, poly-3-hexylthiophene (P3HT) and 6,6'-phenyl-C₆₁ butyric acid methyl ester (PCBM). Small band gap polymers are also used for the donor material to harvest long-wavelength light of the solar radiation spectrum.^{3,4} The conversion efficiency would be determined by several processes, including photoabsorption (exciton generation), exciton diffusion in the donor material, exciton dissociation (charge transfer) at the donor–acceptor heterojunction, and transports of free electron and hole to the electrodes.^{1–13} Understanding these mechanisms at the microscopic level is important to provide design rules for high-efficiency photovoltaics.

Time-resolved spectroscopies of the organic photovoltaics^{2,3,6–10} suggest that the photogenerated exciton decays to an interface polaron at the donor–acceptor heterojunction, which is referred to as the “charge transfer (CT) state”. The CT states have been observed in the photoabsorption spectra of P3HT/PCBM films as a peak below the band gap.^{8,9} The charge transfer occurs within a few hundred femtoseconds.^{2,3,6,7} Subsequently, the localized CT state dissociates into free carriers or decays to the ground state,^{3,6,7} where the latter path reduces the energy conversion efficiency. The charge transfers would be governed by the electronic structure of donor–acceptor interfaces as well as the vibronic coupling (electron–phonon coupling).^{7,11,14–21}

In this study, we theoretically investigate the exciton dissociations at donor–acceptor heterojunctions. We consider donor–acceptor

interfaces comprising an oligothiophene (OT₄) and C₆₀ (panels c–e of Figure 1) as a model system to provide fundamental insights into the exciton dissociations. We analyze the (i) absorption spectra, (ii) electronic structures in adiabatic and diabatic representations, (iii) vibronic coupling, and (iv) quantum dynamics of the charge transfers. The effects of donor–acceptor distance and stacking structure are investigated.

The OT₄/C₆₀ interface is a proper model system of the donor–acceptor heterojunctions that comprise more complicated polymers^{1–9} or oligomers;^{12,13} e.g., the alkyl side chains of P3HT are not essential for the molecular orbitals relevant to the exciton dissociation. The main difference between oligothiophene and polythiophene in terms of the electronic structure is the π -conjugation length, i.e., the longer the π -conjugation length, the lower the exciton energy.

2. METHODS

2.1. Electronic Structures. Density functional theory (DFT) is a practical approach for the electronic structure calculations of large systems such as P3HT/fullerene.^{22,23} In this study, the electronic structures are calculated using the time-dependent DFT with long-range correction (LC-TDDFT).²⁴ The exciton and CT states at the donor–acceptor interface consist of singly excited configurations, which can be described by TDDFT. The most dominant configuration for the exciton is the excitation from the highest occupied molecular orbital (HOMO) to the lowest unoccupied molecular orbital (LUMO) within the donor, and that for the CT state is the excitation from the donor's HOMO to acceptor's LUMO (Figure 1d). The LC-TDDFT is

Received: April 6, 2011

Published: April 29, 2011

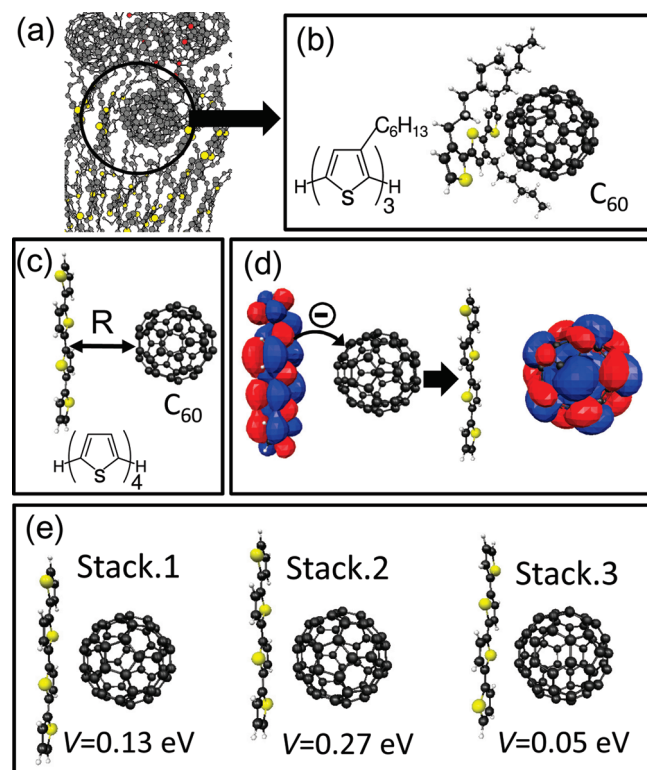


Figure 1. (a) Schematic illustration of a P3HT/PCBM heterojunction. (b) Ground state equilibrium geometry of oligo-hexylthiophene/C₆₀. (c) Model of OT₄/C₆₀ interface, where the five- or six-membered ring (SMR or 6MR) of C₆₀ and the π-conjugate plane of OT₄ are arranged in parallel. (d) Scheme of the electron transfer with the LUMOs of OT₄ and C₆₀. (e) Stacking structures of the OT₄/C₆₀ interface with the exciton-CT coupling, V , at $R = 3$ Å: (Stack.1) a 6MR of C₆₀ faces to the -C=C- bond between thiophene rings; (Stack.2) a 6MR of C₆₀ faces to a thiophene ring; (Stack.3) a SMR of C₆₀ faces to a thiophene ring.

known to describe charge transfers adequately²⁴ and thus is well suited for the present system. The LC-TDDFT calculations were performed using the GAMESS code.²⁵ The BLYP functional^{26,27} and the 31G split basis set with the SBKJC pseudopotential²⁸ were employed.

2.2. Quasi-Diabatization Scheme. We analyze the electronic structures based on the diabatic representation. In practice, the diabatic representation cannot uniquely be defined from the adiabatic states and thus appropriate quasi-diabatization schemes are applied.²⁹ Our quasi-diabatization scheme is briefly summarized as follows.

- We prepare the set of reference wave functions, $\Phi_{\text{ref-}i}$, that possess pure exciton and CT characters.
- We calculate the adiabatic states of the donor–acceptor interface at a given interface structure, for which the intermolecular interaction can induce mixing of exciton and CT characters.
- The diabatic wave functions are represented by a linear combination of adiabatic wave functions, Ψ_i :

$$\Phi_I = \sum_i C_{li} \Psi_i, \quad C_{li} = \langle \Psi_i | \Phi_{\text{ref-}I} \rangle \quad (1)$$

That is, the adiabatic states are considered as basis functions for expanding the diabatic states. This is exact only if the diabatic state, Φ_I , is completely identical to the corresponding reference

wave function, $\Phi_{\text{ref-}I}$. In practice, the accuracy of the quasi-diabatization can be improved by increasing the number of basis adiabatic wave functions. In this study, the reference wave functions were calculated at a sufficiently long intermolecular distance at which the adiabatic states correspond to the pure exciton and CT states. Then for evaluating the overlap between Ψ_i and $\Phi_{\text{ref-}I}$, the intermolecular distance is changed while the eigenvectors of the reference wave functions are fixed. The Slater determinants, i.e., the electron exchanges, are taken into account for correct description of the overlaps. The diabatic potentials and couplings are evaluated from the diabatic wave functions as follows

$$E_1 = \langle \Phi_1 | H | \Phi_1 \rangle, \quad E_2 = \langle \Phi_2 | H | \Phi_2 \rangle \quad (2a)$$

$$V = \langle \Phi_1 | H | \Phi_2 \rangle \quad (2b)$$

where H is the electronic Hamiltonian. This quasi-diabatization scheme is applicable for any ab initio and DFT methods that employ localized basis sets.

2.3. Vibronic Coupling. We analyze the vibronic coupling based on the potential crossing of the diabatic states. We consider the intramolecular vibronic coupling in the harmonic approximation, where the definitions of parameters are similar to those of the Marcus parabola (Figure 4a).¹⁴ The parameters are determined based on the LC-TDDFT calculations. The exciton (XT) and CT potentials are expressed as follows in dimensionless coordinates, where the minimum of the exciton potential is set to zero

$$E_{\text{XT}} = \sum_i \frac{\omega_i}{2} x_i^2 \quad (3a)$$

$$E_{\text{CT}} = \sum_i \frac{\omega_i}{2} x_i^2 + \sum_i \kappa_i x_i - \varepsilon_{\text{XT-CT}}(\text{XT}_{\text{min}})$$

$$\kappa_i = -\Delta x_i \omega_i, \quad \lambda_{\text{XT-CT}} = \sum_i \frac{\kappa_i^2}{2\omega_i} \quad (3b)$$

$$\Delta E = \lambda_{\text{XT-CT}} + \varepsilon_{\text{XT-CT}}(\text{XT}_{\text{min}}) \quad (3c)$$

$$\varepsilon_{\text{XT-CT}}(\text{XT}_{\text{min}}) = \varepsilon_{\text{XT-CT}}(G_{\text{min}}) + \lambda_{\text{G-CT}} - \lambda_{\text{G-XT}} - \lambda_{\text{XT-CT}} \quad (3d)$$

The frequencies of normal modes, ω_i , are calculated at the CT minimum. Since the pure CT diabatic state comprises the OT₄ cation (donor) and the C₆₀ anion (acceptor), we separately calculate the vibrational modes of the donor and acceptor, and we omit the intermolecular vibrations. The vibronic coupling constant, κ_i , of each mode is determined based on the displacement between the XT and CT minima, Δx_i . The reorganization energies among the XT, CT, and ground states ($\lambda_{\text{XT-CT}}$, $\lambda_{\text{G-XT}}$, and $\lambda_{\text{G-CT}}$) are evaluated by geometry optimizations from the vertical transitions (Figure 4a) or by the normal-mode analysis according to the relation of eq 3b. These two ways give almost the same values, meaning that the harmonic approximation is valid for the present system. The energy difference, ΔE , and the XT-CT gap (i.e., $\varepsilon_{\text{XT-CT}} = E_{\text{XT}} - E_{\text{CT}}$) at the XT minimum, $\varepsilon_{\text{XT-CT}}(\text{XT}_{\text{min}})$, are evaluated by the relation of eqs 3c and 3d. Here, $\varepsilon_{\text{XT-CT}}(G_{\text{min}})$ is the XT-CT gap at the ground state

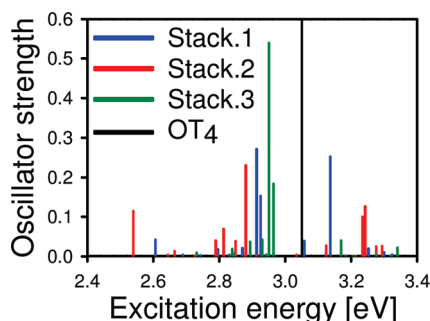


Figure 2. Absorption spectra of the OT₄/C₆₀ interfaces at $R = 3$ Å by the LC-TDDFT calculations. The excitation energy of the isolated OT₄ is also shown.

minimum. ΔE and λ are defined as absolute values, while $\varepsilon_{\text{XT-CT}}$ can have positive or negative values.

The charge transfer rate by the Marcus theory¹⁴ is based on Fermi's golden rule and thus valid for perturbative regimes, i.e., weak diabatic couplings. The Marcus theory is not suitable for ultrafast dynamics, and thus we perform explicit quantum dynamics calculations for the present system that exhibits ultrafast charge transfers.

2.4. Quantum Dynamics. We perform quantum dynamics calculations for the exciton dissociations by solving the following Schrödinger equation (in a.u.) in the diabatic representation using the multiconfiguration time-dependent Hartree (MCTDH) method³⁰

$$i \frac{\partial}{\partial t} \begin{pmatrix} \varphi_{\text{XT}}(\mathbf{X}) \\ \varphi_{\text{CT}}(\mathbf{X}) \end{pmatrix} = \begin{pmatrix} H_{\text{XT}} & V \\ V & H_{\text{CT}} \end{pmatrix} \begin{pmatrix} \varphi_{\text{XT}}(\mathbf{X}) \\ \varphi_{\text{CT}}(\mathbf{X}) \end{pmatrix} \quad (4)$$

Here, $\varphi_{\text{XT}}(\mathbf{X})$ and $\varphi_{\text{CT}}(\mathbf{X})$ are the vibrational wave functions of the exciton and CT states. In the MCTDH method, the vibrational wave functions are described as a linear combination of the Hartree products of single-mode wave functions.³⁰ The vibronic coupling is described by the spin-boson model as follows

$$H_{\text{XT}} = \sum_{i=1}^N \frac{\omega_i}{2} (p_i^2 + x_i^2) \quad (5a)$$

$$H_{\text{CT}} = \sum_{i=1}^N \frac{\omega_i}{2} (p_i^2 + x_i^2) + \sum_{i=1}^N \kappa_i x_i - \varepsilon_{\text{XT-CT}}(\text{XT}_{\min}) \quad (5b)$$

Here, ω_i , p_i , and x_i are the frequency, momentum, and coordinate along each mode, respectively. N is the total number of modes (264 for OT₄/C₆₀). The diabatic coupling, V , and the parameters, κ_i and $\varepsilon_{\text{XT-CT}}$, are determined by the LC-TDDFT calculations as described above. The present Hamiltonian does not account for the intermolecular relaxation, which is in general relatively slow as compared to the intramolecular vibrations. The diabatic coupling is assumed to be independent of the intramolecular vibrations. This assumption is generally reasonable when the intramolecular relaxation is moderate, i.e., does not undergo large structural changes such as bond breakings and isomerizations. At the initial condition, the vibrational wave function is centered at the minimum of exciton potential.

We can reduce the number of vibrational modes while keeping the accuracy of short time dynamics by introducing a hierarchical structure of the electron–phonon coupling.^{17–21,31} The spin boson

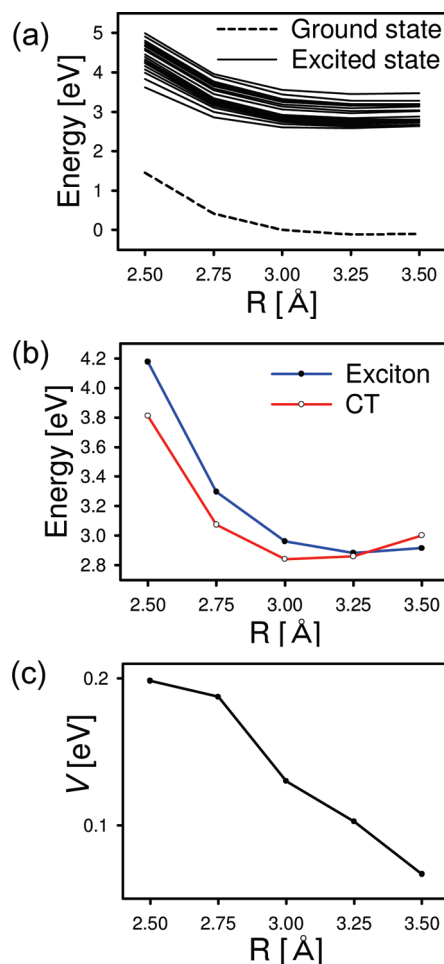


Figure 3. Energy profiles of the (a) adiabatic states, (b) exciton and CT diabatic states, and (c) exciton-CT diabatic coupling, for the Stack.1 as a function of the donor–acceptor distance. The zero of energy is set to the ground state energy at $R = 3$ Å.

model (eq 5) is transformed to the hierarchical electron–phonon (HEP) model by a coordinate transformation as follows^{17–21}

$$H_{\text{HEP}} = \sum_{i=1}^N \frac{\Omega_i}{2} (P_i^2 + X_i^2) + K_1 X_1 + \sum_{i=2}^N d_{i-1,i} (X_{i-1} X_i + P_{i-1} P_i) + \varepsilon_{\text{XT-CT}}(\text{XT}_{\min}) \quad (6)$$

Equations 5 and 6 are formally equivalent. Here, Ω_i , P_i , and X_i are the frequency, momentum, and coordinate after the transformation, respectively. K_1 and d_{ij} are the parameters of the vibronic coupling and the bilinear mode–mode couplings, respectively. While the vibrational modes are coupled via the band-diagonal bilinear coupling terms (the third term), only the X_1 mode directly contributes to the vibronic coupling (the second term). We perform reduced-dimensional quantum dynamics calculations by truncating the vibrational modes in the HEP model. The HEP model was successfully applied for the exciton dissociations at donor–acceptor polymer heterojunctions.^{17–20}

3. RESULTS AND DISCUSSION

There should be various possibilities of the local interface structure depending on the fabrication condition.⁵ As a reference,

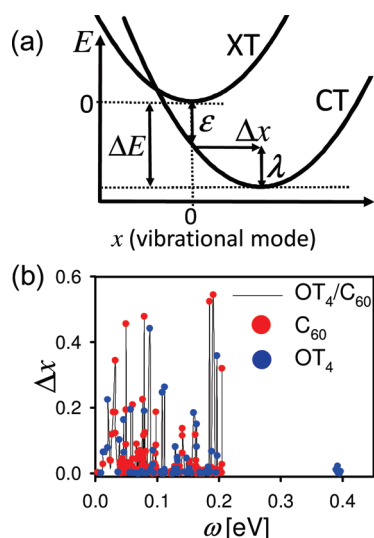


Figure 4. (a) Potential crossing of the exciton (XT) and CT diabatic states in the harmonic approximation. ΔE is the energy difference between the minima of potentials, λ is the reorganization energy, ε is the XT-CT gap, and Δx is the shift of potential. (b) Potential shift along each intramolecular vibrational mode of the C_{60} anion and the OT_4 cation, where ω is the frequency.

we calculate the equilibrium π - π stacking distance between oligohexylthiophene (i.e., small P3HT) and C_{60} (Figure 1b) in the ground state by using the DFT calculations with Grimme's dispersion correction.³² The equilibrium π - π stacking distance is found to be ~ 3 Å, where the C_{60} is wrapped by alkyl side chains as experimentally observed for P3HT/ C_{60} before annealing.⁵ In the following LC-TDDFT calculations of the excited states, Grimme's dispersion correction is not applied.

Figure 2 shows the calculated absorption spectra of three kinds of stacking structures of OT_4/C_{60} at the donor-acceptor distance of 3 Å (Figure 1e), where the excitation energy of isolated OT_4 is shown for comparison. The spectra depend sensitively on the stacking structure, because the donor-acceptor coupling strength depends on the stacking structure. The strong peaks around the excitation energy of 2.7–3.1 eV correspond to the excitonic states of OT_4 in which the CT character is mixed to a certain extent. The weak peaks around 2.5–2.6 eV are mainly of the CT character, but contain some excitonic character. Such an interface polaron below the band gap has been observed in the photoabsorption spectra of P3HT/PCBM.^{8,9} As the exciton-CT mixing increases, the oscillator strength of the interface polaron increases. We calibrate the calculated spectra based on the difference in the excitation energies between OT_4 (~ 3.05 eV) and P3HT (~ 2.21 eV^{8,9}), by which the lowest peak (~ 2.54 eV) shifts to ~ 1.7 eV. This value is similar to the experimental peak of the interface polaron of P3HT/PCBM (~ 1.55 eV).^{8,9}

Figure 3a shows the energy profile of the adiabatic electronic states calculated by the LC-TDDFT as a function of the donor-acceptor distance, where the geometries of OT_4 and C_{60} are fixed at the ground state geometry. These adiabatic states are converted to a diabatic representation for the following analysis. Figure 3b shows the energy profile of the exciton and CT diabatic states of the Stack.1 (Figure 1e). The CT becomes more stable than the exciton as the donor-acceptor distance becomes shorter, owing mainly to the Coulomb interaction. The exciton-CT diabatic coupling, V , becomes stronger as the donor-acceptor distance

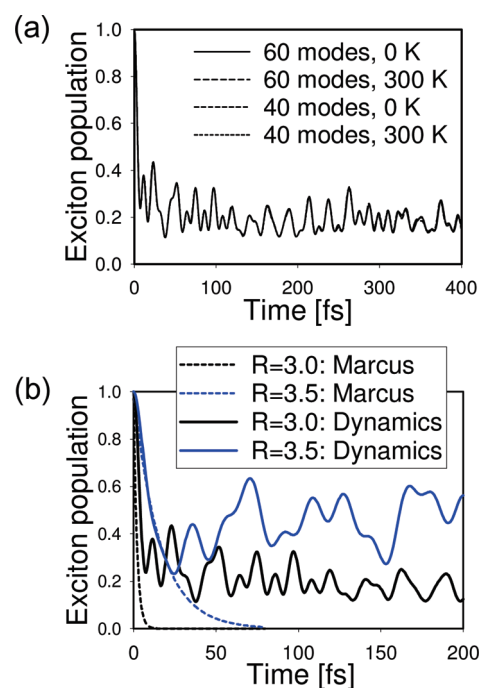


Figure 5. (a) Test of the adequate number of vibrational modes for the quantum dynamics calculations of the exciton decay, as well as the temperature effect, where the parameters for the Stack.1 at $R = 3.0$ Å are used. (b) Exciton decay dynamics using the parameters for the Stack.1 at $R = 3.0$ and 3.5 Å, where 40 vibrational modes are considered and the temperature is 300 K. Exponential decay curves by the Marcus theory are also shown as a reference (dashed lines).

decreases (Figure 3c), reflecting the mixing of the exciton and CT characters in the corresponding adiabatic states. The diabatic coupling also depends on the stacking structure (Figure 1e). The strongest diabatic coupling (~ 0.27 eV) is found for the face-to-face stacking between the thiophene ring and C_{60} six-membered ring (Stack.2 in Figure 1e). For this stacking structure, the oscillator strength of the interface polaron is relatively strong (the peak at ~ 2.55 eV in Figure 2).

The vibronic coupling can play an important role in charge transfers.^{7,11,14–20} We analyze the intramolecular vibronic coupling based on the diabatic representation (Figure 4a), which is parametrized by the LC-TDDFT calculations. The intramolecular reorganization energy, λ_{XT-CT} , from the exciton to CT states of OT_4/C_{60} is found to be ~ 0.13 eV. This value is smaller than the energy difference, ΔE , at the donor-acceptor distance shorter than ~ 3 Å, which is characterized as the Marcus inverted region.¹⁴ A small reorganization energy of fullerene has been experimentally observed, and its importance for the charge transfer has been suggested.¹¹

Figure 4b shows a map of the vibrational energy, ω , vs the shift of the potential minima, Δx , along each mode. The strong peaks around ~ 0.2 eV correspond to the C=S and C=C stretch modes of the OT_4 cation and the C_{60} anion. The low-frequency peaks below ~ 0.1 eV correspond to the in-plane bending modes of the OT_4 cation and the Hg modes of the C_{60} anion.

Finally, we investigate the dynamics of the exciton dissociations. The diabatic coupling of the present system is so strong that the Fermi's golden rule may not be applied for evaluating the transfer rate. Here, we perform quantum dynamics calculations for the exciton dissociations by using the MCTDH method.³⁰

Figure 5a shows the time-evolution of exciton population by the reduced dimensional quantum dynamics calculations of OT₄/C₆₀ based on the HEP model (eq 6), where the 40- and 60-modes models give almost identical results within ~ 400 fs. That is, the 40-modes HEP model is adequate for reproducing the short time dynamics.

The temperature is taken into account by exciting the vibrational modes at the initial condition according to the Planck distribution. In the present system, the average phonon numbers at 300 K are nearly zero except for some low-frequency modes. The dynamics at 300 K is not significantly different from that at 0 K (Figure 5a), because the charge transfer is not a thermally activated process when the diabatic coupling is strong. The ultrafast charge transfer is largely determined by the high-frequency modes, while the role of the intramolecular low-frequency modes, e.g., the Hg modes of C₆₀, is found to be relatively small.

Figure 5b shows the exciton populations in the quantum dynamics calculations for the Stack.1 (Figure 1e) at the donor–acceptor distance of 3 and 3.5 Å. Note that the $\epsilon_{\text{XT-CT}}$, ΔE (Figure 3a), and V depend on the donor–acceptor distance. Exponential decay curves by the Marcus theory are also shown for comparison. The quantum dynamics calculations indicate ultrafast exciton dissociations due to the strong exciton–CT coupling (Figure 5), as observed in the time-resolved spectroscopies of conjugated polymers and fullerenes.^{2,3,6,7} At 3.5 Å distance, the small ΔE (~ 0.007 eV) results in an oscillatory behavior of the population due to back transfers from the CT to exciton states (Figure 5b). At 3 Å distance, the electronic excess energy, ΔE (~ 0.21 eV), rapidly dissipates into the vibrational energy. At this distance, the exciton/CT population ratio settles down around 1/4 after the rapid exciton decay, which indicates the mixed nature of the corresponding adiabatic state. The interface CT state has a certain excitonic character (Figure 2), which would cause a radiative decay to the ground state.

4. CONCLUSIONS

Our quantum dynamics calculations parametrized by the LC-TDDFT calculations exhibit ultrafast exciton dissociations at the OT₄/C₆₀ interfaces owing mainly to the strong exciton–CT coupling. Similar ultrafast exciton decays are also observed for the time-resolved spectroscopies of the heterojunctions of conjugated polymers and fullerenes.^{2,3,6,7} The coupling strength and relative energy between the exciton and CT states depend sensitively on the donor–acceptor distance and the stacking structure, which in turn affects the absorption spectra and the dynamics of exciton dissociations. The experimentally observed properties would reflect the ensemble of various stacking structures, e.g., the orientation of C₆₀ would be flexible at the interface. The equilibrium donor–acceptor distance decreases after the charge transfer (Figure 3b), because the Coulomb interaction stabilizes the CT state. Such relaxation might be unfavorable for the generation of free electron and hole,¹⁰ e.g., trapping to a too deep CT state hinders the carrier generation. Our quantum dynamics calculations imply that the depth of CT state (i.e., ΔE) also influences the energy dissipation (Figure 5b).

One of the important issues to be addressed next is the generation of free carriers from the localized CT state. Finally, we emphasize that the present approach is generally applicable for the analysis of photovoltaics, including the exciton transfers, charge transports, as well as the multistate dynamics from the exciton to free carriers.

AUTHOR INFORMATION

Corresponding Author

*E-mail: hiroyuki@wpi-aimr.tohoku.ac.jp.

Present Addresses

[§]Institute of Physical and Theoretical Chemistry, Goethe University Frankfurt, Max-von-Laue-Strasse 7, 60438 Frankfurt/Main, Germany

ACKNOWLEDGMENT

This study was supported by the grants-in-aid for scientific research (A) from MEXT, Japan.

REFERENCES

- (1) Scharber, M. C.; Mühlbacher, D.; Koppe, M.; Denk, P.; Waldauf, C.; Heeger, A. J.; Brabec, C. J. Design Rules for Donors in Bulk-Heterojunction Solar Cells—Towards 10% Energy-Conversion Efficiency. *Adv. Mater.* **2006**, *18*, 789–794.
- (2) Sariciftci, N. S.; Smilowitz, L.; Heeger, A. J.; Wudi, F. Photo-induced Electron Transfer from a Conducting Polymer to Buckminsterfullerene. *Science* **1992**, *258*, 1474–1476.
- (3) Hwang, I. W.; Soci, C.; Moses, D.; Zhu, Z.; Waller, D.; Gaudiana, R.; Brabec, C. J.; Heeger, A. J. Ultrafast Electron Transfer and Decay Dynamics in a Small Band Gap Bulk Heterojunction Material. *Adv. Mater.* **2007**, *19*, 2307–2312.
- (4) Park, S. H.; Roy, A.; Beaupré, S.; Cho, S.; Coates, N.; Moon, J. S.; Moses, D.; Leclerc, M.; Lee, K.; Heeger, A. J. Bulk Heterojunction Solar Cells with Internal Quantum Efficiency Approaching 100%. *Nat. Photonics* **2009**, *3*, 297–303.
- (5) Yang, C.; Hu, J. G.; Heeger, A. J. Molecular Structure and Dynamics at the Interfaces within Bulk Heterojunction Materials for Solar Cells. *J. Am. Chem. Soc.* **2006**, *128*, 12007–12013.
- (6) Pensack, R. D.; Banyas, K. M.; Barbour, L. W.; Hegadorn, M.; Asbury, J. B. Ultrafast Vibrational Spectroscopy of Charge Carrier Dynamics in Organic Photovoltaic Materials. *Phys. Chem. Chem. Phys.* **2009**, *11*, 2575–2591.
- (7) Pensack, R. D.; Asbury, J. B. Beyond the Adiabatic Limit: Charge Photogeneration in Organic Photovoltaic Materials. *J. Phys. Chem. Lett.* **2010**, *1*, 2255–2263.
- (8) Goris, L.; Poruba, A.; Hodáková, L.; Vaněček, M.; Haenen, K.; Nesládek, M.; Wagner, P.; Vanderzande, D.; Schepper, L. D.; Manca, J. V. Observation of the Subgap Optical Absorption in Polymer-Fullerene Blend Solar Cells. *Appl. Phys. Lett.* **2006**, *88*, 052113.
- (9) Parkinson, P.; Lloyd-Hughes, J.; Johnston, M. B.; Herz, L. M. Efficient Generation of Charges via Below-Gap Photoexcitation of Polymer-Fullerene Blend Films Investigated by Terahertz Spectroscopy. *Phys. Rev. B* **2008**, *78*, 115321.
- (10) Morteani, A. C.; Sreearunothai, P.; Herz, L. M.; Friend, R. H.; Silva, C. Exciton Regeneration at Polymeric Semiconductor Heterojunctions. *Phys. Rev. Lett.* **2004**, *92*, 247402.
- (11) Imahori, H.; Tkachenko, N. V.; Vehmanen, V.; Tamaki, K.; Lemmetyinen, H.; Sakata, Y.; Fukuzumi, S. An Extremely Small Reorganization Energy of Electron Transfer in Porphyrin–Fullerene Dyad. *J. Phys. Chem. A* **2001**, *105*, 1750–1756.
- (12) Sakai, J.; Taima, T.; Saito, K. Efficient Oligothiophene:Fullerene Bulk Heterojunction Organic Photovoltaic Cells. *Org. Electron.* **2008**, *9*, 582–590.
- (13) Nishizawa, T.; Tajima, K.; Hashimoto, K. The Effect of Crystallinity in Donor Groups on the Performance of Photovoltaic Devices Based on an Oligothiophene–Fullerene Dyad. *Nanotechnology* **2008**, *19*, 424017.
- (14) Marcus, R. A. Electron Transfer Reactions in Chemistry. Theory and Experiment. *Rev. Mod. Phys.* **1993**, *65*, 599–610.

- (15) Ramon, J. G. S.; Bittner, E. R. Exciton Regeneration Dynamics in Model Donor–Acceptor Polymer Heterojunctions. *J. Phys. Chem. B* **2006**, *110*, 21001–21009.
- (16) Bittner, E.; Ramon, J. G. S.; Karabunarliev, S. Exciton Dissociation Dynamics in Model Donor-Acceptor Polymer Heterojunctions. I. Energetics and Spectra. *J. Chem. Phys.* **2005**, *122*, 214719.
- (17) Tamura, H.; Ramon, J. G. S.; Bittner, E. R.; Burghardt, I. Phonon-Driven Ultrafast Exciton Dissociation at Donor-Acceptor Polymer Heterojunctions. *Phys. Rev. Lett.* **2008**, *100*, 107402.
- (18) Tamura, H.; Ramon, J. G. S.; Bittner, E. R.; Burghardt, I. Phonon-Driven Exciton Dissociation at Donor-Acceptor Polymer Heterojunctions: Direct versus Bridge-Mediated Vibronic Coupling Pathways. *J. Phys. Chem. B* **2008**, *112*, 495–506.
- (19) Tamura, H.; Bittner, E. R.; Burghardt, I. Nonadiabatic Quantum Dynamics based on a Hierarchical Electron-Phonon Model: Exciton Dissociation in Semiconducting Polymers. *J. Chem. Phys.* **2007**, *127*, 034706.
- (20) Tamura, H.; Bittner, E. R.; Burghardt, I. Exciton Dissociation at Donor-Acceptor Polymer Heterojunctions: Quantum Nonadiabatic Dynamics and Effective-Mode Analysis. *J. Chem. Phys.* **2007**, *126*, 021103.
- (21) Tamura, H. Coherent Transfer via Environment-Induced Vibronic Resonance. *J. Chem. Phys.* **2009**, *130*, 214705–1–8.
- (22) Kanai, Y.; Grossman, J. C. Insights on Interfacial Charge Transfer Across P3HT/Fullerene Photovoltaic Heterojunction from Ab Initio Calculations. *Nano Lett.* **2007**, *7*, 1967–1972.
- (23) Kanai, Y.; Grossman, J. C. Role of Semiconducting and Metallic Tubes in P3HT/Carbon-Nanotube Photovoltaic Heterojunctions: Density Functional Theory Calculations. *Nano Lett.* **2008**, *8*, 908–912.
- (24) Towada, Y.; Tsuneda, T.; Yanagisawa, S.; Yanai, Y.; Hirao, K. A Long-Range-Corrected Time-Dependent Density Functional Theory. *J. Chem. Phys.* **2004**, *120*, 8425–8433.
- (25) Schmidt, M. W.; Baldridge, K. K.; Boatz, J. A.; Elbert, S. T.; Gordon, M. S.; Jensen, J. H.; Koseki, S.; Matsunaga, N.; Nguyen, K. A.; Su, S.; Windus, T. L.; Dupuis, M.; Montgomery, J. A. General Atomic and Molecular Electronic Structure System. *J. Comput. Chem.* **1993**, *14*, 1347–1363.
- (26) Becke, A. D. Density-Functional Exchange-Energy Approximation with Correct Asymptotic Behavior. *Phys. Rev. A* **1988**, *38*, 3098–3100.
- (27) Lee, C.; Yang, W.; Parr, R. G. Development of the Colle-Salvetti Correlation-Energy Formula into a Functional of the Electron Density. *Phys. Rev. B* **1988**, *37*, 785–789.
- (28) Stevens, W. J.; Basch, H.; Krauss, M. Compact Effective Potentials and Efficient Shared-Exponent Basis Sets for the First- and Second-Row Atoms. *J. Chem. Phys.* **1984**, *81*, 6026–6033.
- (29) Subotnik, J. E.; Cave, R. J.; Steele, R. P.; Shenoi, N. The Initial and Final States of Electron and Energy Transfer Processes: Diabatization as Motivated by System-Solvent Interactions. *J. Chem. Phys.* **2009**, *130*, 234102.
- (30) Meyer, H. D.; Manthe, U.; Cederbaum, L. S. The Multi-Configurational Time-Dependent Hartree Approach. *Chem. Phys. Lett.* **1990**, *165*, 73–78.
- (31) Gindensperger, E.; Köppel, H.; Cederbaum, L. S. Hierarchy of Effective Modes for the Dynamics through Conical Intersections in Macrosystems. *J. Chem. Phys.* **2007**, *126*, 034106.
- (32) Grimme, S. Semiempirical GGA-type Density Functional Constructed with a Long-Range Dispersion Correction. *J. Comput. Chem.* **2006**, *27*, 1787–1799.